Title: Numerical modelling of lithosphere-asthenosphere interaction and intraplate deformation in the Gulf of Guinea

Authors:

1. Jaime Almeida (jaime.almeida@segal.ubi.pt, @JaimeEAlmeida1)
2. Hamzeh Mohammadigheymasi
3. Marta Neres
4. Stéphanie Dumont

Numerical modelling of lithosphere-asthenosphere interaction and intraplate deformation in the Gulf of Guinea

Jaime Almeida[1,2*], Hamzeh Mohammadigheymasi[3,4], Marta Neres[5,6], Stéphanie Dumont[6]

[1] SEGAL, Departamento de Informática (UBI), Rua Marquês d'Ávila e Bolama, Covilhã, 6201-0012, Portugal
[2] Instituto Dom Luiz (IDL) - Universidade da Beira Interior, Covilhã, 6201-0012, Portugal
[3] Atmosphere and Ocean Research Institute (AORI), The University of Tokyo, Kashiwa, 277-0882, Japan
[4] Department of Computer Sciences, University of Beira Interior (UBI), Covilhã, 6200-001, Portugal
[5] IPMA, Instituto Português do Mar e da Atmosfera, Rua C do Aeroporto, Lisboa, 1749-077, Portugal
[6] Instituto Dom Luiz (IDL) - Faculdade de Ciências da Universidade de Lisboa, 1749-016, Lisboa, Portugal

*Corresponding author: jaime.almeida@segal.ubi.pt

Abstract

To present day, the phenomenon of intraplate deformation and its associated earthquakes remain elusive. In this work, we argue that intraplate deformation may result from the interaction between lithospheric and upper mantle dynamic processes. To this extent, we targeted the Gulf of Guinea and adjacent Western Africa, a region with both low plate velocities and clear asthenosphere dynamics, allowing us to isolate the individual underlying dynamic constraints which govern intraplate deformation. Thus, here we present 3D numerical geodynamic models of the asthenosphere-lithosphere interaction in the Gulf of Guinea, ran with the state-of-the-art modelling code LaMEM. We employ different initial/boundary conditions such as: (a) identical vs different spreading rates for the varying segments of the Atlantic mid-ocean ridge, (b) the presence/absence of weak zones (e.g., the Romanche/Central-African shear zones), and (c) the effect exerted by an active mantle plume, with a varying ascension velocity. Seismic data was used to evaluate the models and their validity. Our results suggest that intraplate deformation within the Gulf of Guinea is influenced by the spreading rate of the mid-ocean ridge, with stress being localized around the ocean-continent transition and existing shear zones. They also suggest that the existence of an underlying stress source (e.g., a mantle plume) beneath the Cameroon region is crucial to explain the epicenter distribution/deformation in the region.

Keywords

Intraplate deformation; Seismicity; Numerical modelling; Gulf of Guinea

Highlights

- The seismic event distribution in the Gulf of Guinea can be explained by the interaction between two separate stress sources.
- The presence of lithospheric weak zones allows the stress from the mid-ocean ridge to be transferred in-land, with the seismicity in the Southern part of Ghana partly reflecting this process.
- A mantle plume underneath the Cameroon can explain the seismic events in the region.

1. Introduction

Intraplate deformation and associated intraplate earthquakes have been a widely studied problem in the fields of geodynamics and seismology. While most large magnitude earthquakes occur mainly along plate boundaries, some of these major events have occurred in regions usually associated with low stress and/or lack of seismicity (such as along rifted passive margins, e.g. Olugboji et al., 2021). Their occurrence has been explored over the past century, and many scenarios have been proposed to explain them, such as anomalies in the thermal structure of the lithosphere (e.g., Eastern China; Weiran et al., 2009), distribution of local geological structures such as (weak) fault zones (e.g., Bergman and Solomon, 1980; Talwani, 2017), stress buildup (e.g., Calais et al., 2016), far-field stress transmission (e.g., Nkodia et al., 2020), gravitational potential energy (Levandowski et al., 2017; Neres et al., 2018); and/or to deep lithosphere/upper asthenosphere processes (e.g., He and Santosh, 2017; Pysklywec and Cruden, 2004; Wang and Currie, 2017). One region widely affected by intraplate seismicity, both on- and off-shore, is the Sub-Saharian African margin. Along this transform continental margin (e.g., Sykes, 1978; Attoh et al., 2005; Jourdon et al., 2021), there has been a significant amount of in-land seismic events since 1615 (Mohammadigheymasi et al., 2023c), including 73 events of Magnitude >= 5 associated which caused local destruction of infrastructures in the Accra (Ghana). Up to now, no relationship between the local stress fields and pre-existing structures has been provided (Olugboji et al., 2021), despite extensive studies over the past century (see Nkodia et al., 2022 and references therein). To further decipher the origin of this intraplate activity, we explore a possible link between intraplate earthquakes/deformation along the Sub-Saharian African margin and the dynamics of the underlying asthenosphere and upper mantle, specifically along the Gulf of Guinea (GG, see Fig. 1). Within the GG, there are two possible stress sources, with one being the slow spreading of the Mid Atlantic Ridge (MAR, c.a. 5-15 mm/yr, Müller et al., 2008) and its associated compressive/shear stress (Turcotte and Schubert, 2002); while the second can be traced to the possible source of the Cameroon Volcanic Line (CVL). While different hypotheses have been proposed for the formation and maintenance of the CVL (these are extensively explored in Adams, 2022), the present work adopted the working theory of the existence of mantle plume in the region (e.g., Adams, 2022; Celli et al., 2020). Furthermore, we considered two major weak zones, which can act as stress localizers (Willis et al., 2019; Bergman and Solomon, 1980; Talwani, 2017), the Romanche Fracture Zone (Attoh et al., 2004, 2005) and the Central African Shear zone (Plomerová et al., 1993). Using the state-of-the-art geodynamic modelling code LaMEM (Kaus et al., 2016), we developed a set of numerical geodynamical 3D models in which we systematically explored the contribution of the stress sources and weak zones to intraplate deformation in the GG area. Our modelling conditions include the systematic testing of different initial and boundary conditions such as:

- The shear stress induced by the individual spreading ridge segments of the Atlantic mid-ocean ridge. This parameter was controlled by testing identical vs different spreading rates in the individual segments. With identical spreading rates, the oceanic plate is pushed equally toward the continent by each individual ridge segment, inducing identical compressive stresses into the continent. Given this, any heterogeneity will be the result of the geometry/rheology of the continent itself.

- The effects induced by the presence of weak zones (e.g., the Romanche/Central-African shear zones). To evaluate their effective contribution in lithospheric stress distribution, models were run with and without these weak structures while maintaining all other conditions.
- The regional stress changes induced by an encroaching active mantle plume. As with the previous condition, models were run with and without an active mantle plume.

2. Geological and tectonic context

The GG is a region famous for its coastlines, the circum-south Atlantic African coast, which perfectly match the coast of the south-America continent, forming a piece of the continental drift puzzle which contributed to the current theory of plate tectonics (Wegener, 1920; Le Pichon, 1968; Burke et al., 1971). Beyond the geometrical argument, geological and structural evidence based on the correlation between the Pan-African and Brasilian orogenic belts, shear zones and cratons were clearly established (Ledru et al., 1994; Caxito et al., 2020 and references therein) indicating that the two continental blocks were initially part of a same supercontinent, Gondwana. Moreover, these common structures and faciès present in both continents provide additional information on the phases of deformation that predate and participated to the formation of Gondwana dated to 630-500 Ma (Caxito et al., 2020 and references therein). These latter are confined in between the present-day cratons, namely the West Africa and Congo cratons for the African block and the Amazonian and São Francisco cratons for the Brazilian block, and testify of the past presence of oceanic basins, continental magmatism, multiple subduction arcs and orogens which took place between 1000 and 630 Ma (Caxito et al., 2020 and references therein). Thus, along the GG coast, two main suture zones can be found, one along the eastern border of the West Africa craton. It is mainly known as the Dahomeyides belt, which crosses the countries of Ghana, Togo and Benin. A second one, the Central African Orogen, mainly located in Cameroon, borders the northern part of the Congo craton.

The breakup of Gondwana initiated after 250 Ma, was featured by multiple phases of rifting, themselves preceded by plume-related flood volcanism, leading to the progressive opening of the Central and South Atlantic (Fairhead and Green, 1989; Renne et al., 1992; Courtillot et al., 1999). This is during the period between the late stage of orogenes (<590 Ma) and progressive Gondwana breakup that an extensive network of shear zones developed, correlated in space and time with post-collisional granitic magmatism (Fairhead, 1988; Caxito et al., 2020). Among them, the Kandi-Transbrasiliano shear zone represents the main trans-continental structure which extends from the Hoggar region to Ghana in Africa and to the East of the Amazonian craton for the Brasil. The corner of the GG is also featured by several shear zones and their splays, among which the Central African Shear Zone (CASZ) extends from the GG's corner in Cameroon to Darfur region in western Sudan. The GG also features more recent volcanic activity, that of the CVL which initiated about 30 Ma in between the oceanic domain with four islands - Pagalu, São Tomé, Príncipe and Bioko, and the continent domain, forming a 1000 km-long line (Déruelle et al., 1991). The CVL volcanism does not show any clear hotspot-like age progression, partly explaining why several hypotheses on its origin have been proposed (Déruelle et al., 1991; Burke, 2001). Presently, the main volcanic activity of CVL is focused in between Mount Cameroon volcano and Bioko Island (Tabod et al., 1992; DePlaen et al., 2014). As with most intraplate settings, GG shows a rather low seismicity which contrasts with the plate boundary formed by the Mid-Atlantic Ridge to the West of the GG (Meghraoui, 2016; Meghraoui et al., 2019). Despite this, a persistent seismic activity including the occurrence of a Mw>6 earthquake has been recorded in South Ghana. There, the suture zone connects the continental tectonic structures to the oceanic domain with the Romanche fracture zone (Meghraoui et al., 2019; Mohammadigheymasi et al., 2023c and references therein).

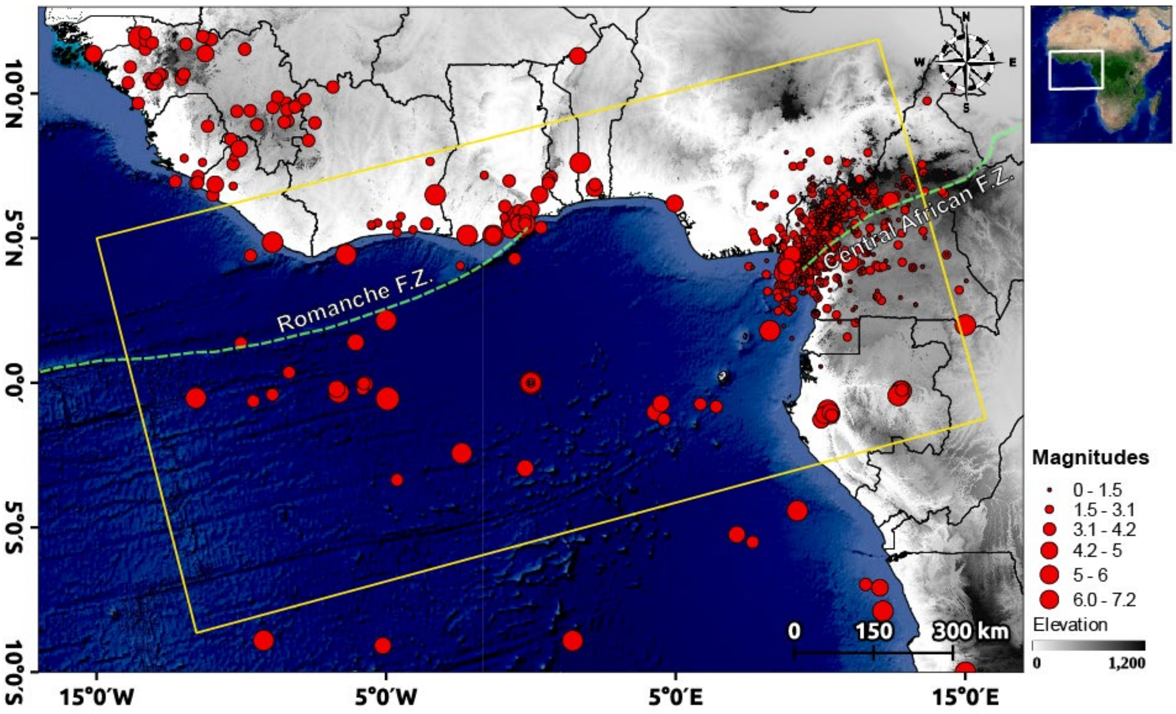

Figure 1: The Gulf of Guinea. Modelled area is highlighted by a light yellow rectangle. Epicenters in the Mid Atlantic Ridge (MAR) are omitted for clearer visualization of MAR's structure. The grayscale background represents a Digital Elevation Model (DEM) provided by NASA Shuttle Radar Topography Mission (SRTM) (2013).

3. Methods

3.1. Data collection

As a tool to validate numerical models, we first compiled relevant existing data characterizing the crustal structure, tectonic features, seismic anisotropy, and seismicity of the GG. This comprehensive compilation draws from various studies and includes data from published papers and data centers. Noteworthy parameters of our research encompass:

- **Crustal thickness, Moho depth, compressed and shear-wave velocities, and crustal stress field**: Of particular significance is the extensive characterization the crustal structure of Nigeria, Ghana, and Cameroon, encompassing information on Vp/Vs and Poisson's ratios, as well as Moho depth. This data has been compiled from the following sources Elsheikh et al. (2014); Custódio et al. (2022); Kamguia et al. (2005); Fairhead and Okereke (1988); Stuart et al. (1985); Tokam et al. (2010); Akpan et al. (2016); Mohammadigheymasi et al. (2023c, 2024).
- **Seismic catalog**: The catalog we compiled integrates various sources, including the comprehensive historical and instrumental catalog assembled by Musson (2014), event reports from the Ghana Geological Survey (GHGS), and data from the International Seismological Center (ISC). Furthermore, it reflects the results of recent efforts to reprocess existing digital seismic data in the GG, utilizing deep learning methods (Mohammadigheymasi et al., 2022, 2023a,b; Carvalho et al., 2023; Mohammadigheymasi et al., 2024). The catalog spans a period from 1615 to 2023, encompassing 1723 earthquakes with moment magnitudes Mw ranging from 1 to 7.2, covering a depth range from 60 km below the Earth's surface up to the surface. A graphical representation of this catalog is provided in Fig. 1.

A summary of the compiled crustal structure, thickness, and average crustal velocity in Cameroon, Ghana, and Nigeria is presented through tables, figures, and a supplementary GIS database. The raw data and GIS datasets are stored in the supplementary GitHub repository of this paper, a link for which is provided in the section 7 – Data Availability.

3.2. Numerical approach

The conducted numerical models were run using the LaMEM code (Kaus et al., 2016), using internally imposed kinematic conditions to simulate the MAR spreading and the Cameroon plume upwelling. No compressibility was assumed for these modelling runs. LaMEM employs a finite difference staggered grid discretization which is coupled with a particle-in-cell approach (Kaus et al., 2016) as to obtain numerical solutions for the conservation equations of mass, momentum, and energy (eq. 1-3)

$$\frac{\partial \mathbf{v_i}}{\partial x_i} = 0 \tag{1}$$

$$-\frac{\partial P}{\partial x_i} + \frac{\partial \boldsymbol{\tau}_{\mathbf{ij}}}{\partial x_j} + \rho \mathbf{g_i} = 0 \tag{2}$$

$$\rho C_p \left(\frac{\partial T}{\partial t} + \mathbf{v_i} \frac{\partial T}{\partial x_i} \right) = \frac{\partial}{\partial x_i} \left(\kappa \frac{\partial T}{\partial x_i} \right) + H_R + H_S \tag{3}$$

Here, i and j are coordinate indexes, $\boldsymbol{v}_i$ represents the velocity vector, x_{ij} the cartesian coordinates, P the pressure, $\tau_{\mathbf{ij}}$ the shear stress, ρ the density, $\mathbf{g}$ the gravitational acceleration vector, Cp the specific heat, T the temperature, t the time, κ the thermal conductivity, and H_R and H_S represent the radiogenic and shear heating components, respectively. The shear heating component is defined as:

$$H_S = \boldsymbol{\tau}_{\mathbf{ij}} \left(\dot{\boldsymbol{\varepsilon}}_{\mathbf{ij}} - \dot{\boldsymbol{\varepsilon}}_{\mathbf{ij}}^{\text{elastic}} \right) \tag{4}$$

with $\varepsilon_{\mathbf{ij}}$ as the total deviatoric strain rate tensor and $\dot{\boldsymbol{\varepsilon}}_{\mathbf{ij}}^{\text{elastic}}$ the deviatoric elastic strain rate tensor.

All presented models were run using non-linear viscoelastoplastic rheology, with the following constitutive equations (Kaus et al., 2016; Piccolo et al., 2020):

$$\dot{\boldsymbol{\varepsilon}}_{\text{ij}} = \dot{\boldsymbol{\varepsilon}}_{\text{ij}}^{\text{viscous}} + \dot{\boldsymbol{\varepsilon}}_{\text{ij}}^{\text{elastic}} + \dot{\boldsymbol{\varepsilon}}_{\text{ij}}^{\text{plastic}} = \frac{\boldsymbol{\tau}_{\mathbf{ij}}}{2\eta_{eff}} + \frac{\mathring{\tau}_{ij}}{2G} + \dot{\gamma} \frac{\partial Q}{\partial \boldsymbol{\tau}_{\mathbf{ij}}} \tag{5}$$

$$\mathring{\tau}_{ij} = \frac{\partial \boldsymbol{\tau}_{\mathbf{ij}}}{\partial t} + \boldsymbol{\tau}_{\mathbf{ik}} \boldsymbol{\omega}_{\mathbf{kj}} - \boldsymbol{\omega}_{\mathbf{ki}} \boldsymbol{\tau}_{\mathbf{kj}} \tag{6}$$

$$\boldsymbol{\omega}_{\mathbf{ij}} = \frac{1}{2} \left(\frac{\partial \mathbf{v_j}}{\partial x_i} - \frac{\partial \mathbf{v_i}}{\partial x_j} \right) \tag{7}$$

with η_{eff} as the effective viscosity, $\mathring{\boldsymbol{\tau}}_{\boldsymbol{ij}}$ the Jaumann objective stress rate, $\boldsymbol{\omega}_{\mathbf{ij}}$ the spin tensor, G the elastic modulus and Q the plastic flow potential.

The creep viscosity, η_{vs}, is calculated as:

$$\eta_{vs} = \frac{1}{2} A^{-\frac{1}{n}} \times \dot{\varepsilon}_{II}^{\frac{1}{n}-1} \times \exp\left(\frac{E_a + V_a P}{nRT} \right) \tag{8}$$

with A as the diffusive or dislocation pre-exponential factor, n the stress exponent, $\dot{\varepsilon}_{II}$ the square root of second invariant of the deviatoric strain rate tensor (eq. 5), E_{a} the activation energy, V_a the activation volume and R the gas constant.

Plastic flow is ensured by employing a Drucker-Prager yield criterion (Drucker and Prager, 1952):

$$\sigma_Y = C\cos(\phi) + P\sin(\phi) \tag{9}$$

with σ_Y as the yield stress tensor, ϕ the internal friction angle and C the cohesion. The onset of plastic weakening takes place once mantle materials accumulate at least 10% of total plastic strain and this effect halts after at least 60% of total plastic strain has been accumulated. During softening, the materials' cohesion and internal friction angles are linearly reduced until they reach 1% of their initial values. The effective viscosity (η_{eff}) of the individual phases is obtained by calculating the minimum between the calculated viscoelastoplastic viscosity and the Newtonian viscosity.

The second invariant of the stress tensor (σ_{II}) is obtained as follows:

$$\sigma_{II} = \sqrt{\frac{1}{2}\sigma_{ij}^{\prime\,2}} \tag{10}$$

in which $\sigma_{ij}^{\prime\,2}$ is the sum of the square of all individual deviatoric stress tensor components.

The age dependence of the thermal profiles of the plates follows the half-space cooling model:

$$T = T_{surface} + (T_{mantle} - T_{surface}) \times \mathrm{erf}(\frac{y}{\sqrt{\kappa t}}) \tag{11}$$

Here, $T_{surface}$ represents the temperature at the surface of the model (273 K), T_{mantle} is the temperature at the lithosphere-asthenosphere boundary (1523 K), y the depth, κ the thermal diffusivity, and t the age of the plate. The effective (rheological) lithosphere thickness throughout the model is set by the 1523 K (1250 °C) isotherm. The upper mantle thermal profile follows the mantle adiabat, with a gradient of 0.5 K/km. All material densities are temperature and pressure dependent:

$$\rho = \rho_0 + \alpha(T - T_0) + \beta(P - P_0) \tag{12}$$

Here, $\rho_0$is the density of the material at the reference temperature T_0, α is the thermal expansibility and β is the compressibility. All rheological parameters can be found in Table 1.

The calculation of the modelled stress regime follows the approach defined in Delvaux et al. (1997), by calculating a ration (R) between the primary components of the stress tensor ($\sigma_1, \sigma_2, \sigma_3$).

$$R = \frac{\sigma_2 - \sigma_3}{\sigma_1 - \sigma_3} \tag{13}$$

This ration is then used to calculate a stress index (R') which is defined based on the primary stress directions as follows:

$$\begin{cases} R' = R \quad\quad, & \sigma_1\ vertical \\ R' = 2 - R, & \sigma_2\ vertical \\ R' = 2 + R, & \sigma_3\ vertical \end{cases} \tag{14}$$

The specific stress regime is based on the value obtained for R' with $R' \in [0,1]$ describing extensive, $R' \in]1,2[$ strike-slip, and $R' \in [2,3]$ compressive conditions, respectively.

3.3. Initial setup and modelling approach

A set of 3D models were performed to simulate the kinematics of the sub-Saharan African margin. To assess the influence of the individual controlling factors, we systematically increased the complexity of our models by adding one factor per model, resulting in a total of four exploration models. We ran an additional model in which we test a mid-ocean ridge with no spreading rate variability along the individual segments, as well as a model with a wider plume head, for a total of six models (see Table 2).

The prescribed model domain was 3200 km long, 1500 km wide and 710 km thick (see Fig. 2) and was discretized along a 384x192x128 resolution grid, resulting in a c.a. 8x8x6 km cell. This resolution allowed us to prescribe two of the major weak zones present in the Gulf of Guinea (namely, the Romanche and Central African Shear zones, see Fig. 2) and ensure they have a minimum width of 16 km. The model included a 50 km thick sticky-air layer which acts as a free surface, allowing for the formation of topography. Furthermore, the top boundary is open, ensuring free movement of this layer. All other model boundaries were defined as free slip, which allows for motion along the direction of the boundary but not across it.

Table 1 – Physical parameters applied in the models, for each of the different phases. UC - (Continental) upper crust, LC - (Continental) lower crust. Creep and thermal parameters for the oceanic and upper mantle phases adapted from Kohlstedt et al. (1995), Ranalli and Karato (1995), and Ranalli (1997). Creep and thermal parameters for the continental phases from Ranalli and Karato (1995). Elastic parameters from Kaus et al. (2015). Plastic flow parameters from Ranalli and Karato (1995) and Ranalli (1997) and Li et al. (2010).

		Continent		Oceanic Crust	Upper Mantle
Properties	Parameters	UC	LC		
Density	ρ_0 - kg/m^3	2800	3000	3000	3300
Dislocation creep	B_n - Pa^{-n}/s^{-1}	6.40x10^{-6}	3.30x10^{-4}	2.50x10^{4}	2.50x10^{4}
	n	2.40	3.20	3.5	3.5
	E_n - J/MPa/mol	1.56x10^{5}	2.38x10^{5}	5.30x10^{4}	5.30x10^{4}
	V_n - m^3/mol	0	0	1.35x10^{-5}	1.35x10^{-5}
Diffusion creep	B_I - Pa^{-n}/s^{-1}	-	-	1.50x10^{9}	1.50x10^{9}
	n	-	-	1	1
	E_I - J/MPa/mol	-	-	3.75x10^{5}	3.75x10^{5}
	V_I - m^3/mol	-	-	1.35x10^{-5}	1.35x10^{-5}
Plastic flow	Cohesion - MPa	20	20	30	30
	Softened cohesion - MPa	0.2	0.2	0.3	0.3
	ϕ - degrees	6.8	6.8	20	20
	Softened ϕ - degrees	0.068	0.068	0.2	0.2
Elasticity	G - Pa	5.00x10^{10}	5.00x10^{10}	5.00x10^{10}	5.00x10^{10}
Thermal	Expansivity (α) - 1/K	3x10−5	3x10−5	3x10−5	3x10−5

Properties	Compressibility (β) – Pa^{-1}	$1x10^{-11}$	$1x10^{-11}$	$1x10^{-11}$	$1x10^{-11}$
	Conductivity (κ) - W/m/k	3	3	3	3
	Heat capacity - J/kg/K	1050	1050	1050	1050
	Radiogenic heat production – W/kg	$5.36x10^{-10}$	$2.32x10^{-10}$	$6.67\ x10^{-12}$	$6.67x10^{-12}$

Table 2: List of models run in the present study

Model number	Active ridge	Active plume	Weak zones	Additional constraints
1	Yes	No	No	-
2	Yes	No	Yes	-
3	Yes	No	No	No ridge segment variability
4	Yes	Yes	No	-
5	Yes	Yes	Yes	
6	Yes	Yes	Yes	Wider plume head

The rheology of the oceanic crust follows a dry olivine creep law (Ranalli, 1997) and had a variable thickness which depended on its distance to the spreading ridge centre (half-space cooling model, eq. 10). The lithospheric mantle also follows a dry olivine creep law and differs in behaviour from the crustal material due to a higher temperature (eq. 8).

Our modelled African continent was internally divided into blocks, each with a specific crust thickness and lithospheric mantle thicknesses, which was obtained from geophysical studies (see references in Section 2.1). For simplicity, we assumed that the crust is vertically divided into equally thick upper and lower crust. We assumed a quartzitic creep (Ranalli and Karato, 1995; Ranalli, 1997) and plastic flow (Li et al., 2010) laws for the materials of the upper crust continental. This setting reproduces the overall heterogeneous nature of continental crust, allowing for a weak/brittle upper crust. The lower crust was assumed to follow a stronger plagioclase creep/plastic flow (Ranalli, 1995), ensuring a more consistent stress/strain delocalization and replicating the well-established jelly-sandwich rheological model for continental lithosphere (Burov, 2011).

The internal dynamics of the model are controlled by pre-imposed kinematic conditions, such as the spreading rate of the individual ridge segments along the MAR as well as the injection rate of the high temperature materials of the Cameroon Plume. The geometry and kinematics of the MAR are simulated by implementing four independent kinematically divergent zones, with variable spread rates (see Fig. 2 and Table 3). Each segment is laterally offset from the previous as to favour the establishment of orthogonal transform faults between them and to depict at best the dynamics and related stress distribution of the Atlantic basin for the GG region. The Cameroon plume was modelled by implementing an injection point at the bottom boundary of the model, in which hotter material is added at a constant rate over time. The composition of the plume material was assumed to be identical to the surrounding mantle (see Table 1) but, due to a positive buoyancy (derived from a thermally lowered density), it is forced to ascend. While the specific geometry of this plume cannot be predicted from the start, we imposed a width of 50 km for the stem and an injection velocity of 20 cm/yr. This ensured that the plume head reaches the base of the lithosphere at approximately the same place as in nature (see Fig. 2) when accounting for the spreading rate of the MOR.

The weak zones implemented (which represent two major fault zones present in the region, the Romanche and Central African Shear Zones, see Fig. 1) were defined by an isoviscous rheology (i.e., with a constant low viscosity) of 10^{19} Pa·s as to achieve high strain localization.

Table 3 – Right and left spreading rates in the simulated ridge segments. The segments are identified in Fig. 2-A. Here, positive spreading rate values indicate a spread towards the continent. Conversely, negative values indicate towards the wall.

Segment	Left spreading rate (cm/yr)	Right spreading rate (cm/yr)
1	-	0.50
2	-0.50	1.00
3	-1.25	1.25
4	-1.20	1.20

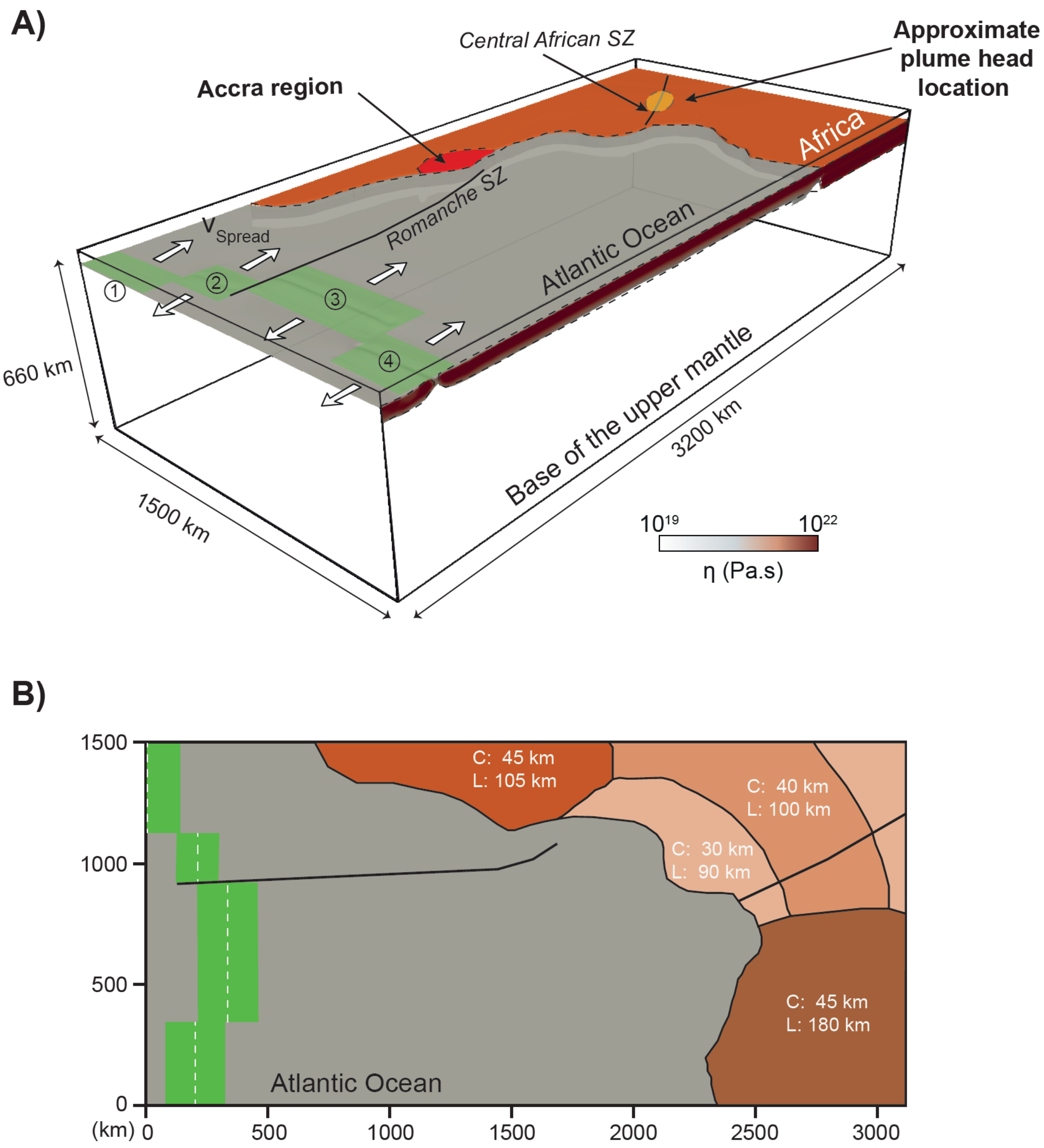

Figure 2: A. Model setup for the experimental initial state: schematic representation of the geometric configuration and model dimensions. The placement of the plume head is approximate and follows previous descriptions (Burke, 2001). The viscosity scale applies only to the front-facing wall. The numbered green polygons mark the position of the individual ridge segments, with their spreading direction indicated by the white arrows. Their half-spreading rates can be found in Supplementary Table A.2. The depth indicated along the z axis does not include the 50 km thick sticky air layer. **B. Continental crustal and lithospheric thicknesses**: the different shaded regions indicate the individual cratonic regions present in our model. Crustal thickness data was described in Section 2.1. Lithospheric thickness from Globig et al. (2016).

4. Results

In this work, we investigated the role of MAR, the two major weak zones (see Fig. 1) and the CVL plume as well as that of their possible interplay in the stress distribution and transfer within the GG. We depart from a simple reference model (Model 1) where only the MAR is active. Then, we incrementally added complexity in subsequent iterations. This ensured that any detected variation would be explained by the added component. In both the single and dual stress source models, two major phases can be defined in which the same broadly defined events occur, namely: Phase 1) establishment of the mid-ocean ridge, and Phase 2) stress migration away from the ridge and towards the continent (see Figs. 3 and 4). An additional phase is seen in the single source models which entails the development of combined continent-ocean deformation.

4.1. Phase 1 – Ridge establishment

In all models (regardless of the type and number of stress sources), the first 0.3 Myr consisted of the establishment of the spreading centers along the ridge. During this time period, stress is almost exclusively confined to these extensional structures (see Figs. 3 and 4, left-most column). Although all models show similar results, the models with pre-existing weak zones (models 2, 5 and 6, in Figs. 3 and 4) show a lower stress accumulation at the MAR at this stage. Furthermore, these same models also show a pronounced stress localization zones both in the ocean-continent transition (OCT) zone and within the continent, with the former showing higher stress values (compare in Figs. 3 and 4 the top with the middle rows).

4.2. Phase 2 – Deformation migration

Once the ridge system is established ($\Delta t > 0.3$ Myr, middle columns in Fig. 3), stress begins to be transmitted to the more distant oceanic plate. Additionally, we also observe incipient stress localization within the continent, specifically in and around the thinner continental blocks (see Fig. 2, with the thicker regions still showing low to no stress accumulation).

The addition of pre-existing weak zones directly affects both the stress distribution and migration velocity. Under their effects (Model 2, middle row in Fig. 3), not only does stress localize quicker within the continent, but it is also maintained for a longer period, with distinct higher stress regions being observed for the rest of the model.

Finally, when the individual segments of the MOR have identical spreading rates (Model 3, Fig. 3, bottom row), the stress propagation in the oceanic plate appears to be less efficient, with the latter model showing overall lower stress values, with more pronounced stress contrasts within the continent (compare in Fig. 3 the top and bottom rows). Nevertheless, both Model 1 and 3 show the same tendency towards the homogenization of stress within the continent, as opposed to the formation of stress bands shown in Model 2. In the models with two stress sources, this phase coincides with the arrival of the plume head to the base of the lithosphere, as observed in Fig. 4. In all three of these models, the plume encroaches the base of the lithosphere, straining it the base of the lithosphere (see Fig. 5), which effectively lowers the viscosity at this location (note in Fig. 4 the lower viscosity values above the 1000°C line). The surface expression of this plume arrival, however, is not identical for all scenarios. We can observe in Fig. 4 that while the two models with pre-established weak zones show some surface expression of the plume arrival, the model without weak zones does not. In addition, this surface expression is more pronounced in the model with a wider mantle plume head.

4.3. Phase 3 – Combined ocean-continent deformation

This last phase is observed in the models with a single stress source (i.e., Fig. 3), taking place after 2 Myr of model time. After this period, we observe the establishment of the final stress localization sites, which appear to be controlled by the presence of the weak zones. When these are not present, stress distribution shows a tendency towards homogenization within the continent, where only relatively weak stress contrasts are seen along craton boundaries (see in Fig. 3 the top and bottom rows). By contrast, weak zones allow for the maintenance of stress localization sites which are still observable within the continent. These sites appear along the weak zone tips, as well as along the boundaries of the cratons (see Fig. 3, middle row).

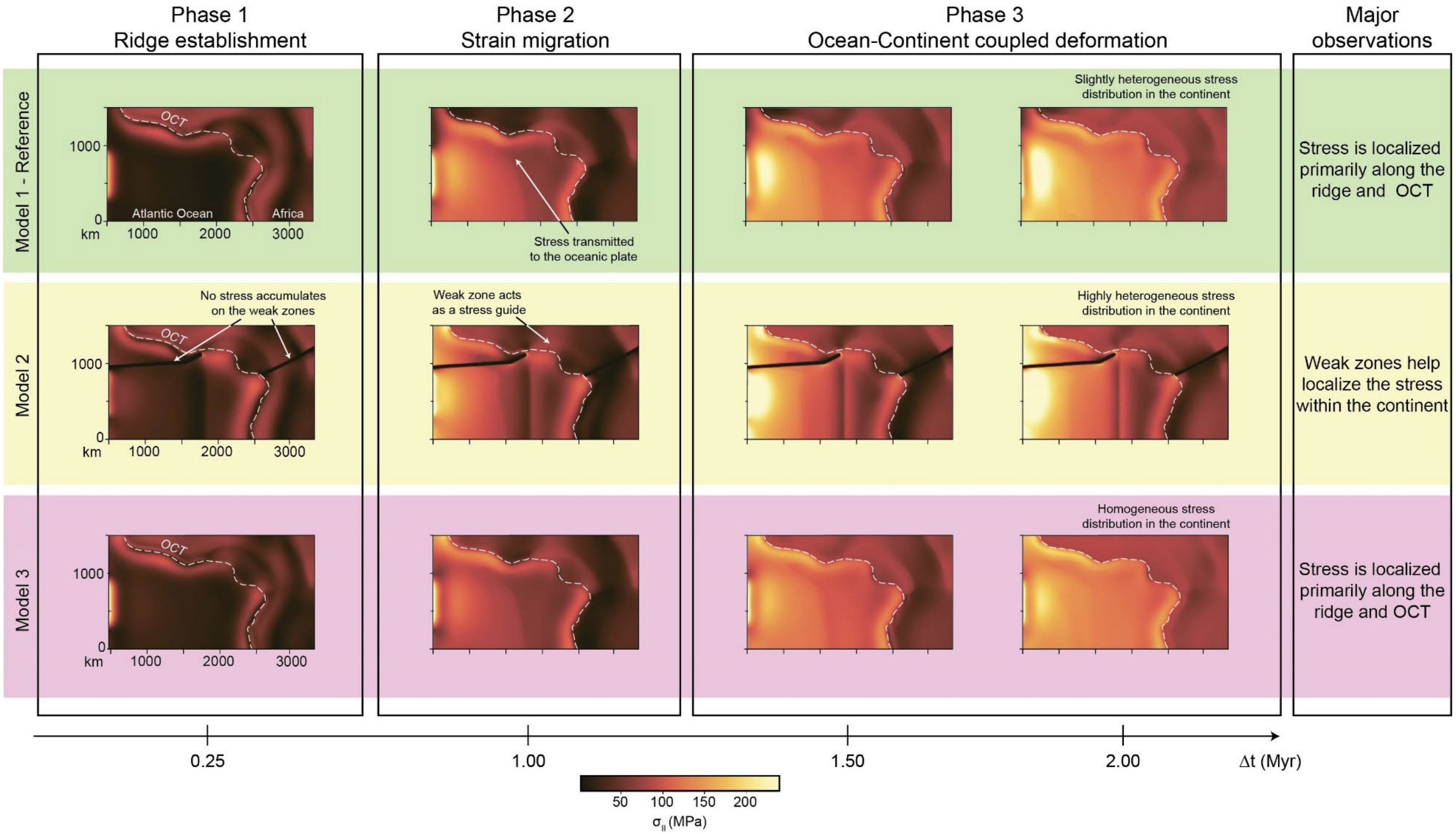

(See caption in the next page)

Figure 3: Major phases and events observed in the single stress source models in terms of deviatoric stress (σ_{II}) distribution. Each column of figures corresponds to identical model times, while each row describes the evolution of a specific model. The right-most column summarizes the key observations for each model. Phase 1 (left-most column) shows first-order identical stress distributions between the three models, with Model 2 (middle row) showing a more effective dissipation of the ridge stress (lower overall $\boldsymbol{\sigma_{II}}$). The same is mostly observed in Phase 2 (second column to the left), in which all models show a simple an increase of stresses within the oceanic plate and, in the case of Model 2, increased stresses within the continent. Lastly, Phase 3 shows a more advanced stage of the system evolution, highlighting the major differences between the three models: both models 1 and 3 show the eventual establishment of (mostly) homogeneous stress distribution in the continent while, by contrast, Model 2 shows a heterogeneous stress state. The white dashed line represents the transition between the ocean and the continent, or OCT. Difference from reference model can be found in Supplementary Fig. 1.

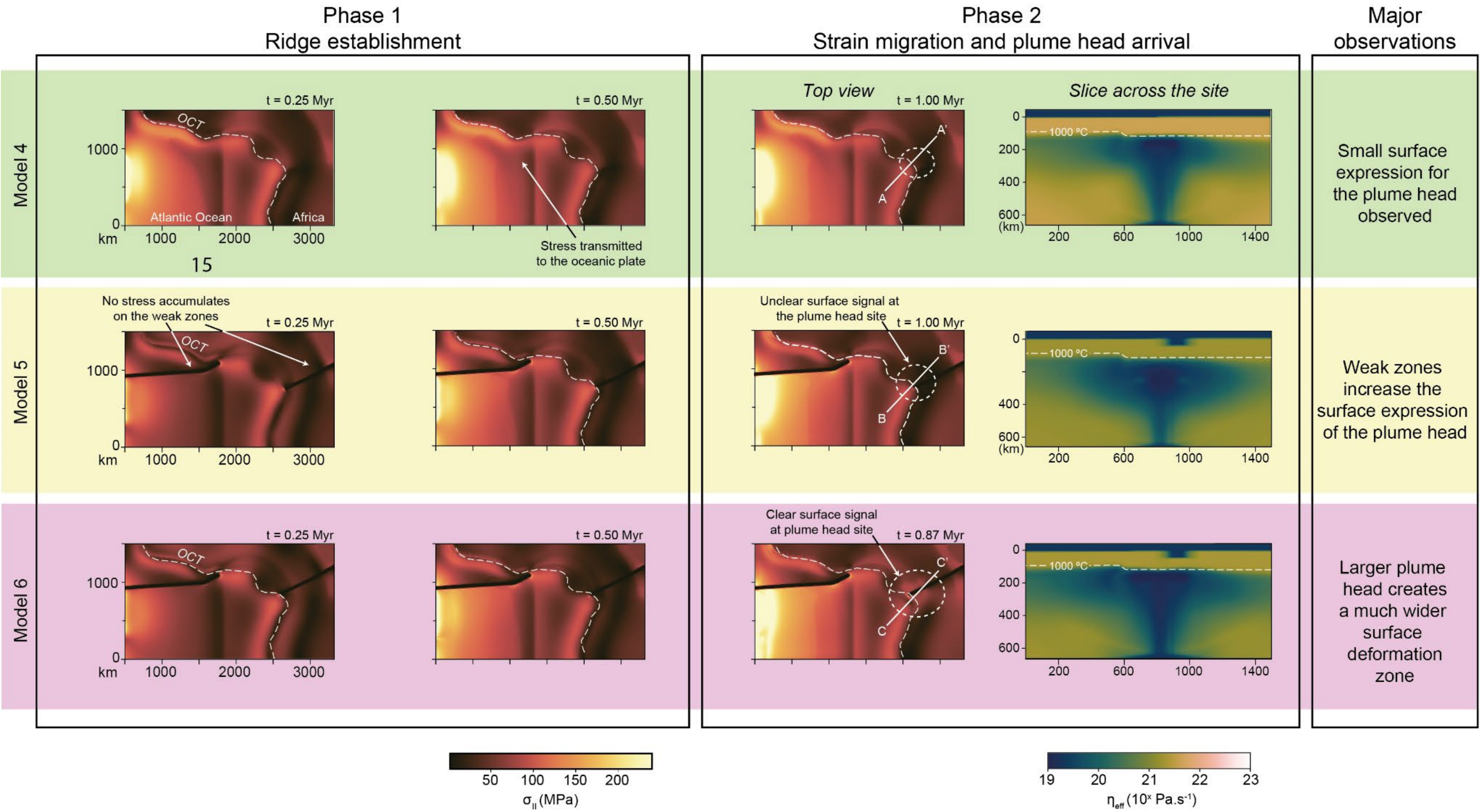

(See caption in the next page)

Figure 4: Major phases and events observed in the dual stress source models in terms of deviatoric stress (σ_{II}) distribution. The three left columns of figures correspond to identical model evolution stages (specific model time is indicated for each), while each row describes the evolution of a specific model. In Phase 1 (two left-most columns), the model results are broadly similar to the ones shown in Fig. 3, with the models with weak zones showing more effective stress dissipation at the ridge (lower overall $\boldsymbol{\sigma_{II}}$ values). In Phase 2, the plume has arrived at the base of the lithosphere in all three models (see the right column in Phase 2, showing a cross section across the plume site). The surface expression of this plume is a function of both the size of the plume head and the presence of weak zones, as (a) only the models with weak zones show any surface expression (middle and bottom rows), and (b) this expression is much more pronounced in the model with a wider plume (bottom row). The white dashed line represents the transition between the ocean and the continent, or OCT. Difference from reference model can be found in Supplementary Fig. 1.

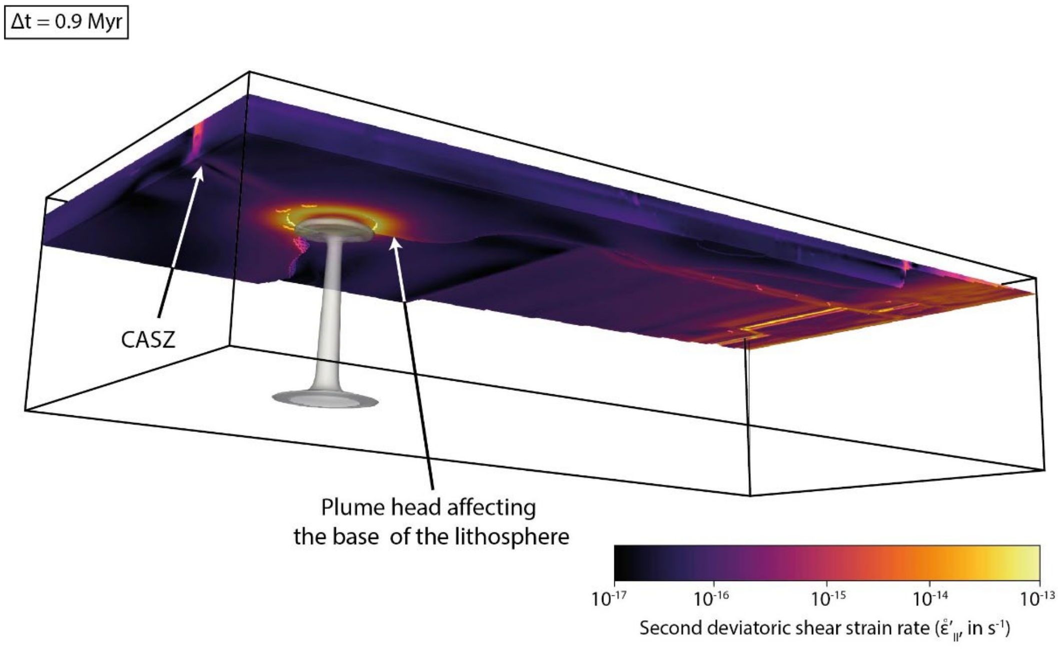

Figure 5: Side view of model 6, after a model time of 0.9 Myr. Here, we observed that a wide high strain ring formed around the top of the plume head. This provided a strong indication that the base of the lithosphere was under a strong strain induced by the arrival of the plume head. Furthermore, by observing the left side of the figure, we also observed that the entirety

of the Central African shear zone (CASZ) is also affected, showing relatively higher strain values along its path. The plume contour is done by mapping the 1700°C isotherm.

5. Discussion

To better decipher the processes leading to the intraplate seismicity and deformation in the GG, our approach consisted of: 1) evaluating the role of the oceanic lithosphere in the stress distribution in the GG region and especially at OCT; and 2) independently test the effect of two sources of stress, namely the MAR and the Cameroon Plume.

5.1. Single stress source

In the models in which the MAR was the sole stress source (i.e., Fig. 3, models 1 and 3), we observe a homogeneous low stress state within the modelled African continent. While these stress states can generate complex strain distributions, when applied in heterogeneous media (e.g., Gerya, 2009), our simulated African continent assumes a constant (i.e., homogeneous) composition with only age differences. Thus, under present modelling conditions, most of the stress will be localized along rheological boundaries, such as the OCT and cratonic boundaries, following the observations of prior studies on deformation of continental lithosphere (e.g., Vauchez et al., 1998; Calignano et al., 2015).

The addition of weak zones in this system has a considerable effect in the stress distribution (compare in Fig. 3, models 1 and 2). Along the ridge-distal tip of our modelled Romanche shear zone, we can observe a significant increase of the stress within the oceanic and continental domains, as well as clear stress contrast along the cratonic boundaries in the region (boundaries shown in Fig. 2). This in-land stress propagation is consistent with previous transform margin modelling studies in which the formation and development of moderately oblique transform faults induces deformation in the continent (e.g., Jourdon et al., 2021). While the low stress within the weak zone (see Fig. 3, Model 2) indicates that the majority of the deformation is being accommodated here, the differential stress along the tip would likely induce the activation of the numerous smaller scale existing fault zones in the region, an effect which has been suggested to be in effect in a prior study of the deformation in Ghana (Nkodia et al., 2020).

5.2. Dual stress source

The addition of an active mantle plume beneath the Cameroon region (see Fig. 2) represented an additional stress source in the system. A comparison between models 1 and 4 revealed that this new stress source produces little-to-no difference on the overall σ_{II} within the continent after 1 Myr (compare the top rows in Figs. 3 vs 4), which suggests that, under present modelling conditions, it might not represent a significant change in the system. However, mantle plumes have been shown to induce both short- and large-scale stress changes both at the surface (e.g., Wang and Li, 2021; Burov and Guillou-Frottier, 2005) and at the base of the lithosphere (e.g., Gedamu et al., 2023). Thus, some additional component was required to obtain the expected surface expression of the plume head. To that extent, we found that the addition of large-scale continental weak zones significantly contributed towards the magnification of plume surface expression, while oceanic based weak zones contributed towards the in-land propagation of the stress along their tips (as previously detailed). Despite the plume head being constrained to the Cameroon region (Fig. 4), it is affecting a much wider region, derived from the thermal weakening of the base of the lithosphere (Fig. 4, right column), but also separating the continent into a north and south domain by the CASZ. By having this precisely placed weak boundary, the plume is able easily force the two regions to spread apart, increasing the surface expression. The widespread weakening by the plume effectively increases the rheological contrast to the east of the Accra region, which in turn leads to a more efficient localization of stress along the cratonic boundary (e.g., Vauchez et al., 1998; Calignano et al., 2015). This effect is also a function of plume head width, as after an identical model time, model 6 shows a much wider surface expression when compared to Model 5 (see Fig. 4).

5.3. Implications for the observed intraplate deformation and seismicity

Within the GG, the seismic activity is mostly concentrated in two major clusters (see Fig. 1), namely the Accra and Cameroon clusters, as well as some scattered events within the Atlantic plate. To evaluate our model results we use two approaches, namely by comparing: (1) the modelled regions of high stress (as shown in Figs. 3 and 4) with the epicenter distribution within the GG (e.g., Mohammadigheymasi et al., 2023c); and (2) between the established deformation regimes for the Gulf of Guinea (e.g. Nkodia et al., 2022) and the modelled deformation regimes.

It has been shown in previous sections that in the scenarios in which the MAR is the only stress source, that most of the available stress localizes along the ocean-continent transition area, forming an envelope around the continental region (see Fig. 3). While this stress distribution could explain the seismic events within the oceanic plate, we argue that even though geological formations are various in this part of the African continent, they are not associated with strong enough rheological contrasts to explain the 2 seismic clusters.

Prior studies in region concerning the origin of the Accra cluster have proposed that these events could be related to either the western Saint Paul FZ and isostatic motions (e.g., Attoh et al., 2005), or to the presence of the Romanche FZ (e.g., Kutu, 2013). We tested the latter hypothesis through Model 2, where we assessed the efficiency of two large-scale weak zones at nucleating stress. As described in a previous section, the addition of the Romanche FZ was enough to induce a pronounced heterogeneity within this region of African continent which can be correlated with a pre-existing rheological boundary (namely a transition between two different continental blocks, corresponding to a suture zone, see Fig. 2-B). The location of this in-land stress propagation also broadly correlates to the location of active structures in the region (see Fig. 6-A and B). Given these results, we argue that it is likely that the Romanche FZ participates in inducing the reactivation of pre-existing structures around Accra, such as the Dahomeyides belt (see Fig. 1), which would explain the observed seismicity in this region. In addition, despite the presence or absence of the Romanche FZ, all models predict the occurrence of broadly compressive to transpressional stress conditions for ocean-continent transition within this region of the GOG (see Area 1 in Fig. 7-A and 7-B, as well as Supplementary Figure 2). Furthermore, as these localized transitions from compressive to transpressive are associated with concavities in the shoreline, it suggests that that the geometry of the continental margin can play a pivotal role in the distribution of the stress regimes in the area. Both observations are consistent with prior studies on the deformation within the GOG (e.g., Nkodia et al., 2022). However, as in Model 2 no increased stress was observed within the Cameroon region, it suggests that the MAR and weak zones alone are insufficient to explain both seismic clusters within the GG, reinforcing the idea of the role played by the OCT geometry.

One of the currently working hypotheses for the formation of the CVL is a complex interaction between the CASZ and an upper mantle plume (e.g., Adams, 2022). Although yet unconfirmed, the region beneath Cameroon has shown to have some of the signatures of a mantle plume, such as a low shear wave velocity which may correspond with an anomalously high thermal signature (e.g., Celli et al., 2020) and OIB-style isotopic signatures (e.g., Tanyileke et al., 1996). Independently of the source of the CVL mantle plume, we aimed at investigating the influence of a (local) thermal anomaly in the distribution of stress in the surrounding/region. Under these constraints, both models 5 and 6 show the emergence of a large high stress zones centered around the plume head, as well as a tendency towards extensive stress regimes within the vicinity of the CASZ (see Fig. 4 and Fig. 7). This high stress region could participate in redistributing stress in a wider region than that directly influenced by the current active centres of the CVL within the Cameroon cluster (see Fig. 6-C), but the localized extension (see Fig. 7-B) and thermal anomaly itself (see Fig. 5) could also help to explain the volcanic activity. One can note that the present-day magmatic and volcanic activity is confined in between Mt Cameroon area and Bioko island, with earthquakes as deep as 50-55 km (Ekodo et al 2023; DePlaen et al 2014). Despite located in this volcanic area, the alignment detected for some seismic events with regional fault systems, attest of complex magmato-tectonic interaction, which could be enhanced in this sector by processes of various origin, as suggested by our models.

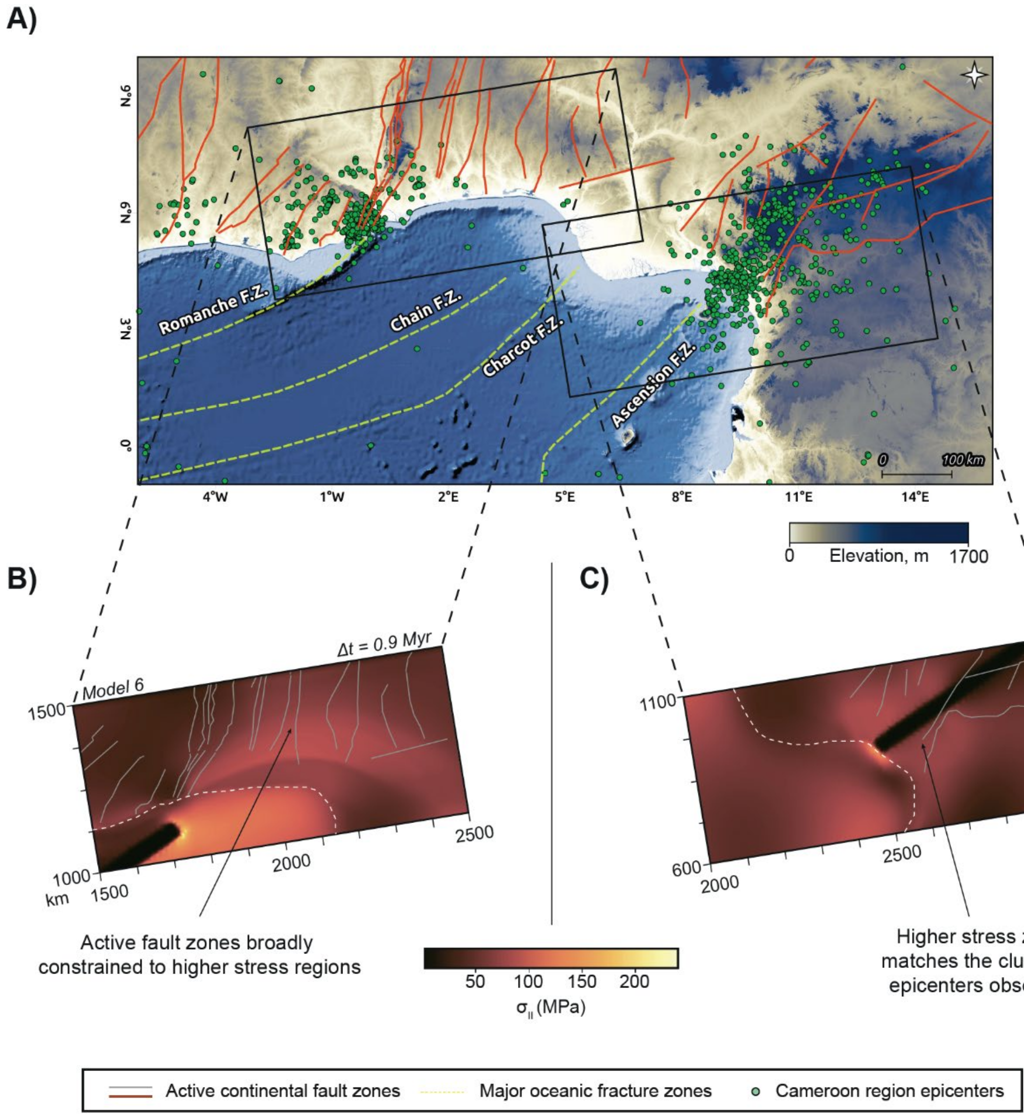

Figure 6: A. Detail map of the target comparison region. This map shows the target area to be used as a comparison with the model results, including both the Accra and Cameroon regions. **B. Model inset of the Accra Region.** Within this model region, it is shown that the active continental fault zones (marked in grey) fall at first order within the higher stress bands. **C. Model inset of the Cameroon region.** This model region, located just above the plume head (as detailed in Fig. 5), shows a large high stress region around the tip of the CASZ, which globally engulfs most of the epicenters found in and around Cameroon.

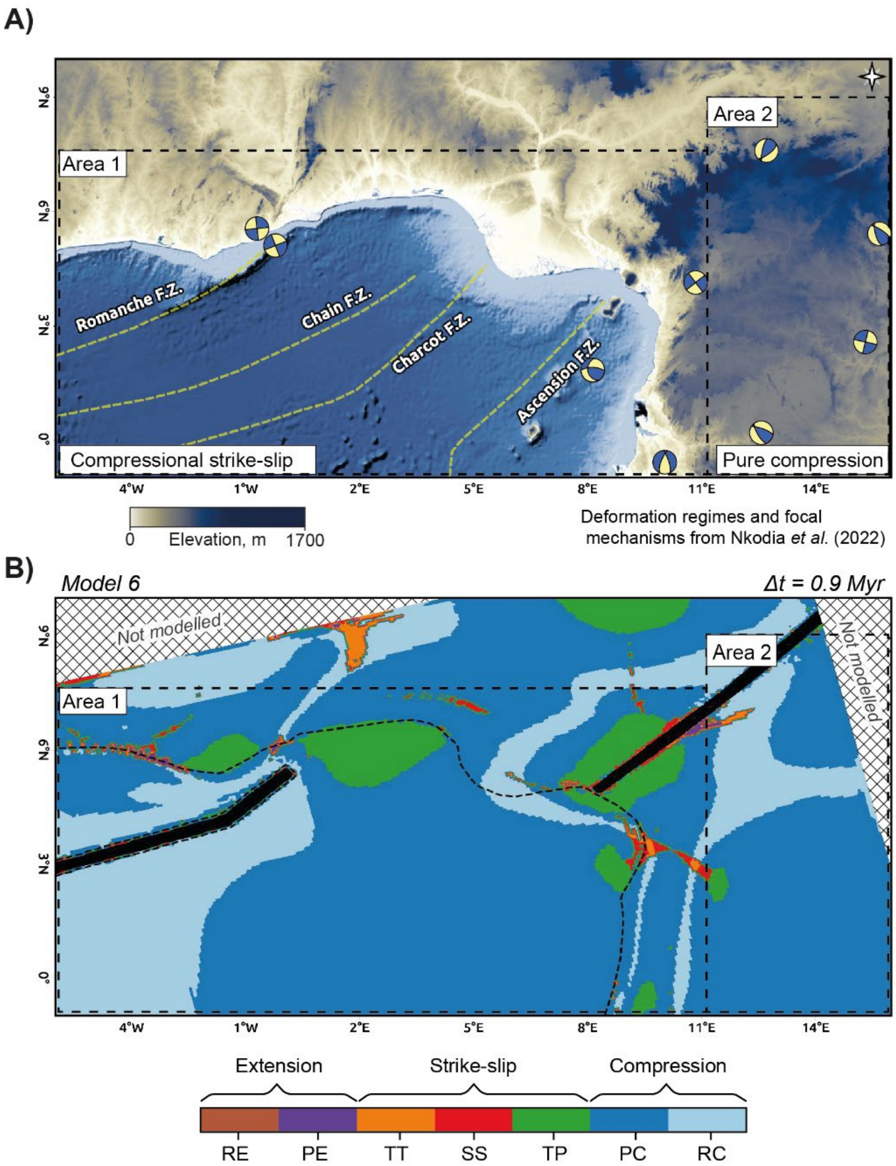

Figure 7: A. Detail map of the target comparison region. This map shows the target area that is compared with the model results and which includes stress regime domains and known focal mechanisms (both from Nkodia et al., 2022). **B) Calculated stress regime conditions for Model 6.** The model shows a prevalence of mostly compressive stress conditions throughout, with highly localized strike-slip/extensional conditions (e.g., around the plume head and in the junction between the Romanche FZ and the continent). These conditions show a good first-order agreement with the known natural stress regimes for the GG, despite local mismatches due to minor (and not modelled) structures. Due to their inherent highly mobile nature, the internal regions of the weak zones show random distributions of stress regimes and, thus, have been blacked out. FZ: fracture zone; RE: radial extension; PE: pure extension; TT: transtension; SS: pure strike-slip; TP: transpression; PC: pure compression; and RC: radial compression.

5.4. Model limitations

The presented models provide insight on the drivers for intraplate deformation and seismicity within the GG. Nevertheless, as with most numerical models, the observations made must take into consideration the limitations of the models and the data quality and coverage.

A first limitation pertains to an uncertainty regarding the condition selection characterizing the rheology of the upper mantle (e.g. Jain and Korenaga, 2020; King, 2016, and references therein). Given this, while there is some liberty regarding the choice if rheological parameters (such as the ones presented in Table A.1), it should be expected that slight variations of these parameters could lead to different results. One possible example of these changes may be effective viscosity of the ascending plume materials which could, for instance, rise faster or slower through the mantle and/or form a narrower/wider plume head beneath the lithosphere. Another parameter which may impact the results is the geothermal gradient. Different thermal profiles would influence the deformation and stress pattern for the different region and sub-regions modelled. Although our thermal profiles are approximated to a continental geotherm, a colder continental lithosphere would result in a stronger prevalence of compressive regimes (an additional model with the initial geometry of Model 2 but older initial lithosphere was run, the results of which can be found in Supplementary Fig. 3).

Secondly, these models do not represent the full extent of the structural complexity of the region as, for instance, we limit our weak zones to that of the CASZ and the Romanche SZ. While there are other large transform faults in the region (e.g., the Ascension SZ), none has the proximity and connection to the known in-land deformation as the Romanche. Thus, only the latter was implemented. It is however plausible that the addition of the St. Paul SZ would increase stresses west of Accra and add further stresses along the Dahomeyides belt. Furthermore, the size of the continental blocks (as well as their thicknesses) used in this work are of first-order and do not reflect the real complexity of the African continent. Nevertheless, our objective was to provide a first order approach concerning the role of the major features on stress localization

Additionally, the models presented in this work do not employ two-phase flow. Mantle plumes are known to induce partial melting within the lithosphere (e.g., Manglik and Christensen, 2006), which not only introduces a liquid phase into the system but also weakens the local rheology (e.g., Whattam and Stern, 2015). A weaker rheology implies that the stress needed to induce deformation is also lower which, therefore, would further imply that a lower stress accumulation would be seen above the plume site. Furthermore, the ascension of the plume in the model is controlled by the interplay between constant injection velocity at the base of the model and thermally lowered density, while in nature the positive buoyancy of the plume is the more important controlling factor. While our imposed injection velocity is in line with the estimated rates for mantle plumes, it is likely that the combined effect of the two factors may be resulting in an exaggerated velocity. In short, it is possible that our models present an overestimation of the accumulated stress above the plume site but are likely observing an underestimation of the deformation in this region.

Finally, one limitation of this work is the identification of possible seismogenic sources and processes in this region. This poor constraint stems from the natural complexity of intraplate settings (discussed in Talwani, 2014), as well as sparse instrumental coverage (Ahulu and Danuor, 2015). Thus, there may be a mismatch between the real distribution of seismicity (both in space and time) and the one shown in the present work, which could compromise our interpretation.

6. Conclusions

With this work, we investigated how the interplay between two major stress sources (i.e., the MAR and a possible Cameroon mantle plume) and large-scale weak zones can explain the intraplate deformation and seismic event distribution within the Gulf of Guinea region using a geodynamic modelling approach.

Our results (as shown in Figs. 3 and 4) suggest that, within the GG, stress distribution can be explained by the contribution of at least two stress sources: the MAR, which contributes to transfer stresses along the OCT and the mantle plume, which localizes stresses in the continental lithosphere in its direct vicinity.

They further suggest that large-scale weak zones are crucial for transferring stress in-land from the MAR, allowing for intraplate stress to accumulate in the continent, following prior field studies in the region such as Nkodia et al., (2022). This leads us to suggest that the maintained seismicity in the sector of Accra results from a complex interaction between MAR, weak fracture zones and OCT, while the seismicity observed in Cameroon, appears to be mainly related to magmatism including active volcanism, and tectonics in the predominantly in the continental domain.

7. Acknowledgements

This work was developed under the frame of the SHAZAM project with the reference PTDC/CTA/GEO/31475/2017; POCI-01-0145-FEDER-031475, co-financed by FEDER-COMPETE/POCI 2020. This work was supported by the European Union and the Instituto Dom Luiz (IDL) Project under Grant UIDB/50019/2020, and it uses computational resources provided by C4G (Collaboratory for Geosciences) (Ref. PINFRA/22151/2016). JA acknowledges support from FCT through project GEMMA (PTDC/CTA-GEO/2083/2021). MN acknowledges support from FCT through project LISA (PTDC/CTA-GEF/1666/2020).

The authors would like to thank Nicolas Riel for his help on solving stability issues with the numerical models, João Fonseca for early and fruitful discussions on the topic and his role in the funding of SHAZAM project, as well as Luísa Cartaxo and Nasrin Tavakolizadeh for the help in making some of the figures shown in the manuscript. The authors also thank the editor Claire Curie, Will Levandowski and an anonymous reviewer for their insightful and constructive comments which have significantly improved our manuscript

8. Data Availability

The raw data and GIS datasets for the compiled crustal structure, thickness, and average crustal velocity in Cameroon, Ghana, and Nigeria can be accessed at https://github.com/SigProSeismology/Crustal-data-Gulf-of-Guinea.git. The raw model output can be found at https://doi.org/10.17605/OSF.IO/6S4QD.

References

Adams, A., 2022. Insights Into the Source of Magmatic Hot-Lines: Forty Years of Geophysical Studies of the Cameroon Volcanic Line. Frontiers in Earth Science 10, 139. doi:10.3389/FEART.2022.838993/BIBTEX.

Ahulu, S., Danuor, S.K., 2015. Ghana's experience in the establishment of a national digital seismic network observatory. Journal of Seismology 19, 667–683. doi:10.1007/s10950-015-9486-z.

Akpan, O., Nyblade, A., Okereke, C., Oden, M., Emry, E., Julià, J., 2016. Crustal structure of nigeria and southern ghana, west africa from p-wave receiver functions. Tectonophysics 676, 250–260. doi: 10.1016/j.tecto.2016.02.005.

Attoh, K., Brown, L., Guo, J., Heanlein, J., 2004. Seismic stratigraphic record of transpression and uplift on the Romanche transform margin, offshore Ghana. Tectonophysics 378, 1–16. doi:10.1016/j.tecto.2003.09.026.

Attoh, K., Brown, L., Haenlein, J., 2005. The role of Pan-African structures in intraplate seismicity near the termination of the Romanche fracture zone, West Africa. Journal of African Earth Sciences 43, 549–555. URL: https://www.sciencedirect.com/science/article/pii/S1464343X05001317, doi:10.1016/j.jafrearsci.2005.09.006.

Bergman, E.A., Solomon, S.C., 1980. Oceanic intraplate earthquakes: Implications for local and regional intraplate stress. Journal of Geophysical Research 85, 5389–5410. doi:10.1029/JB085iB10p05389.

Burke, K., 2001. Origin of the cameroon line of volcano-capped swells. Journal of Geology 109, 349–362. doi:10.1086/319977.

Burke, K., Dessauvagie, T., Whiteman, A., 1971. Opening of the Gulf of Guinea and Geological History of the Benue Depression and Niger Delta. Nature Physical Science 233, 51–55. doi:10.1038/physci233051a0.

Burov, E., Guillou-Frottier, L., 2005. The plume head–continental lithosphere interaction using a tectonically realistic formulation for the lithosphere. Geophysical Journal International 161, 469–490. URL: https://onlinelibrary.wiley.com/doi/abs/10.1111/j.1365-246X.2005.02588.x

Burov, E.B., 2011. Rheology and strength of the lithosphere. Marine and Petroleum Geology 28, 1402–1443. https://doi.org/10.1016/j.marpetgeo.2011.05.008

Calais, E., Camelbeeck, T., Stein, S., Liu, M., Craig, T.J., 2016. A new paradigm for large earthquakes in stable continental plate interiors. Geophysical Research Letters 43, 10,621–10,637. doi:10.1002/2016GL070815.

Calignano, E., Sokoutis, D., Willingshofer, E., Gueydan, F., Cloetingh, S., 2015. Strain localization at the margins of strong lithospheric domains: Insights from analog models. Tectonics 34, 396–412. URL: https://onlinelibrary.wiley.com/doi/abs/10.1002/2014TC003756, doi:10.1002/2014TC003756.

Carvalho, L., Mohammadigheymasi, H., Crocker, P., Tavakolizadeh, N., Moradichaleshtori, Y., Fernandes, R., 2023. Earthquake Detection and Location in the Cameroon Temporary

Network Data Using Deep Learning. Technical Report. Copernicus Meetings. Doi: 10.5194/egusphere-egu23-16438

Caxito, F.d.A., Santos, L.C.M.d.L., Ganade, C.E., Bendaoud, A., Fettous, E.H., Bouyo, M.H., 2020. Toward an integrated model of geological evolution for NE Brazil-NW Africa: The Borborema Province and its connections to the Trans-Saharan (Benino-Nigerian and Tuareg shields) and Central African orogens. Brazilian Journal of Geology 50. doi:10.1590/2317-4889202020190122.

Celli, N.L., Lebedev, S., Schaeffer, A.J., Gaina, C., 2020. African cratonic lithosphere carved by mantle plumes. Nature Communications 11. doi:10.1038/s41467-019-13871-2.

Courtillot, V., Jaupart, C., Manighetti, I., Tapponnier, P., Besse, J., 1999. On causal links between flood basalts and continental breakup. Earth and Planetary Science Letters 166, 177–195. doi:10.1016/S0012-821X(98)00282-9.

Custódio, S., Mohammadigheymasi, H., Tavakolizadeh, N., Matias, L., Silveira, G., 2022. Seismicity analysis of southern Ghana ii: Updated crustal velocity model and hypocentral parameters, in: EGU General Assembly Conference Abstracts, pp. EGU22–5570. Doi: 10.5194/egusphere-egu22-5570

DePlaen, R.S., Bastow, I.D., Chambers, E.L., Keir, D., Gallacher, R.J., Keane, J., 2014. The development of magmatism along the Cameroon Volcanic Line: Evidence from seismicity and seismic anisotropy. Journal of Geophysical Research: Solid Earth 119, 4233–4252. doi:10.1002/2013JB010583.

Déruelle, B., Moreau, C., Nkoumbou, C., Kambou, R., Lissom, J., Njonfang, E., Ghogomu, R.T., Nono, A., 1991. The Cameroon Line: A Review, in: Magmatism in Extensional Structural Settings. Springer Berlin Heidelberg, Berlin, Heidelberg, pp. 274–327. doi:10.1007/ 978-3-642-73966-8_12.

Drucker, D., Prager, W., 1952. Soil Mechanics and Plastic Analysis or Limit Design. Quarterly of Applied Mathematics 10, 157–165. doi:10.1090/qam/48291.

Elsheikh, A.A., Gao, S.S., Liu, K.H., 2014. Formation of the cameroon volcanic line by lithospheric basal erosion: Insight from mantle seismic anisotropy. Journal of African Earth Sciences 100, 96–108. doi: 10.1016/j.jafrearsci.2014.06.011.

Ekodo, J. M. M., Yem, M., Atangana, J. Q. Y., Koah, S. P., & Ekodeck, G. E. (2023). Characteristics of the Mount Cameroon seismicity for the 2005–2015 period (Cameroon, West-Central Africa). Journal of Seismology, 27(1), 95-114. doi:10.1007/s10950-022-10128-2

Fairhead, J., Okereke, C., 1988. Depths to major density contrats beneath the west african rift system in nigeria and cameroon based on the spectral analysis of gravity data. Journal of African Earth Sciences (and the Middle East) 7, 769–777. doi: 10.1016/0899-5362(88)90018-8

Fairhead, J.D., 1988. Late Mesozoic rifting in Africa. Developments in Geotectonics 22, 821–831. doi:10.1016/B978-0-444-42903-2. 50038-5.

Fairhead, J.D., Green, C.M., 1989. Controls on rifting in Africa and the regional tectonic model for the Nigeria and East Niger rift basins. Journal of African Earth Sciences (and the Middle East) 8, 231–249. doi:10.1016/S0899-5362(89)80027-2.

Gedamu, A.A., Eshagh, M., Bedada, T.B., 2023. Lithospheric Stress Due to Mantle Convection and Mantle Plume over East Africa from GOCE and Seismic Data. Remote Sensing 15, 462. URL: https://www.mdpi.com/2072-4292/15/2/462 , doi:10.3390/rs15020462. number: 2 Publisher: Multidisciplinary Digital Publishing Institute.

Gerya, T., 2009. Introduction to Numerical Geodynamic Modelling. Cambridge University Press, Cambridge. doi:10.1017/CBO9780511809101.

Globig, J., Fernàndez, M., Torne, M., Vergés, J., Robert, A., Faccenna, C., 2016. New insights into the crust and lithospheric mantle structure of Africa from elevation, geoid, and thermal analysis. Journal of Geophysical Research: Solid Earth 121, 5389–5424. URL: http://doi.wiley.com/10.1002/2015JB012608, doi:10.1002/2016JB012972.

He, C., Santosh, M., 2017. Intraplate earthquakes and their link with mantle dynamics: Insights from P-wave teleseismic tomography along the northern part of the North–South Tectonic Zone in China. Comptes Rendus Geoscience 349, 96–105. doi:10.1016/J.CRTE.2017.04.002.

Jain, C., Korenaga, J., 2020. Synergy of Experimental Rock Mechanics, Seismology, and Geodynamics Reveals Still Elusive Upper Mantle Rheology. Journal of Geophysical Research: Solid Earth 125, e2020JB019896. doi:10.1029/2020JB019896.

Jourdon, A., Kergaravat, C., Duclaux, G., Huguen, C., 2021. Looking beyond kinematics: 3D thermo-mechanical modelling reveals the dynamics of transform margins. Solid Earth 12, 1211–1232. URL: https://se.copernicus.org/articles/12/1211/2021/, doi:10.5194/se-12-1211-2021.

Kamguia, J., Manguelle-Dicoum, E., Tabod, C., Tadjou, J., 2005. Geological models deduced from gravity data in the garoua basin, cameroon. Journal of Geophysics and Engineering 2, 147–152. doi: 10.1088/1742-2132/2/2/009

Kaus, B.J.P., Popov, A.A., Baumann, T.S., Pusok, A.E., Bauville, A., Fernandez, N., Collignon, M., 2016. Forward and Inverse Modelling of Lithospheric Deformation on Geological Timescales. NIC Series 48, 978–3.

King, S.D., 2016. Reconciling laboratory and observational models of mantle rheology in geodynamic modelling. Journal of Geodynamics 100, 33–50. doi:10.1016/j.jog.2016.03.005.

Kutu, J.M., 2013. Seismic and Tectonic Correspondence of Major Earthquake Regions in Southern Ghana with Mid-Atlantic Transform-Fracture Zones. International Journal of Geosciences 04, 1326–1332. doi:10.4236/ijg.2013.410128.

Le Pichon, X., 1968. Sea-floor spreading and continental drift. Journal of Geophysical Research 73, 3661–3697. doi:10.1029/jb073i012p03661.

Li, Z.H., Gerya, T.V., Burg, J.P., 2010. Influence of tectonic overpressure on P-T paths of HP-UHP rocks in continental collision zones: Thermomechanical modelling. Journal of Metamorphic Geology 28, 227–247. https://doi.org/10.1111/j.1525-1314.2009.00864.x

Ledru, P., Johan, V., Milési, J.P., Tegyey, M., 1994. Markers of the last stages of the Palaeoproterozoic collision: Evidence for a 2 Ga continent involving circum-South Atlantic provinces. Precambrian Research 69, 169–191. doi:10.1016/0301-9268(94)90085-X.

Levandowski, W., Zellman, M., Briggs, R., 2017. Gravitational body forces focus North American intraplate earthquakes. Nature Communications 8, 14314. doi:10.1038/ncomms14314.

Manglik, A., Christensen, U.R., 2006. Effect of lithospheric root on decompression melting in plume-lithosphere interaction models. Geophysical Journal International 164, 259–270. URL: doi:10.1111/j.1365-246X.2005.02811.x.

Meghraoui, M., 2016. The Seismotectonic Map of Africa. Episodes 39, 9–18. doi:10.18814/epiiugs/2016/v39i1/89232.

Meghraoui, M., Amponsah, P., Bernard, P., Ateba, B., 2019. Active transform faults in the gulf of guinea: Insights from geophysical data and implications for seismic hazard assessment. Canadian Journal of Earth Sciences 56, 1398–1408. doi:10.1139/cjes-2018-0321.

Mohammadigheymasi, H., Shi, P., Tavakolizadeh, N., Xiao, Z., Mousavi, S.M., Matias, L., Pourvahab, M., Fernandes, R., 2023a. Ipiml: A deep-scan earthquake detection and location workflow integrating pair-input deep learning model and migration location method. IEEE Transactions on Geoscience and Remote Sensing 61, 1-9. doi:10.1109/TGRS.2023.3293914.

Mohammadigheymasi, H., Tavakolizadeh, N., Matias, L., Mousavi, S.M., Moradichaloshtori, Y., Mousavirad, S.J., Fernandes, R., 2023b. A data set of earthquake bulletin and seismic waveforms for ghana obtained by deep learning. Data in brief 47, 108969. Doi: 10.1016/j.dib.2023.108969

Mohammadigheymasi, H., Tavakolizadeh, N., Matias, L., Mousavi, S.M., Silveira, G., Custódio, S., Dias, N., Fernandes, R., Moradichaloshtori, Y., 2023c. Application of deep learning for seismicity analysis in Ghana. Geosystems and Geoenvironment 2, 100152. doi:10.1016/j.geogeo.2022.100152.

Mohammadigheymasi, H., Tavakolizadeh, N., Mousavi, S.M., Silveira, G., Fernandes, R., 2022. Seismicity analysis in southern Ghana: Detecting local earthquakes by deep learning, in: EGU General Assembly Conference Abstracts, pp. EGU22–5860. Doi: 10.5194/egusphere-egu22-5860

Mohammadigheymasi, H., Xiao, Z., Mousavi, S.M., Jamalreyhani, M., Almeida, J., Garcia, N.M., 2024. Enhanced insight into Ghana's Seismicity through a Refined Crustal Velocity Model and Earthquake Focal Mechanisms. Technical Report. Copernicus Meetings. Doi: 10.5194/egusphere-egu24-8852

Müller, R.D., Sdrolias, M., Gaina, C., Roest, W.R., 2008. Age, spreading rates, and spreading asymmetry of the world's ocean crust. Geochemistry, Geophysics, Geosystems 9, 1–19. doi:10.1029/2007GC001743.

Musson, R., 2014. The seismicity of ghana. Bull. Earthq. Eng. 12, 157–169. NASA Shuttle Radar Topography Mission (SRTM), 2013. Shuttle radar topography mission (srtm) global. distributed by opentopography. URL: https://www.fdsn.org/networks/detail/GH/, doi:doi.org/10.5069/G9445JDF.

Neres, M., Neves, M.C., Custódio, S., Palano, M., Fernandes, R., Matias, L., Carafa, M., Terrinha, P., 2018. Gravitational Potential Energy in Iberia: A Driver of Active Deformation in High-Topography Regions. Journal of Geophysical Research: Solid Earth 123, 10,277–10,296. doi:10.1029/2017JB015002.

Nkodia, H.M.D.V., Miyouna, T., Kolawole, F., Boudzoumou, F., Loemba, A.P.R., Bazebizonza Tchiguina, N.C., Delvaux, D., 2022. Seismo-genic Fault Reactivation in Western Central Africa: Insights From Regional Stress Analysis. Geochemistry, Geophysics, Geosystems 23, e2022GC010377. doi:10.1029/2022GC010377.

Nkodia, H.V., Miyouna, T., Delvaux, D., Boudzoumou, F., 2020. Flower structures in sandstones of the Paleozoic Inkisi Group (Brazzaville, Republic of Congo): Evidence for two major strike-slip fault systems and geodynamic implications. South African Journal of Geology 123, 531–550. doi:10.25131/sajg.123.0038.

Olugboji, T., Shirzaei, M., Lu, Y., Adepelumi, A.A., Kolawole, F., 2021. On the Origin of Orphan Tremors and Intraplate Seismicity in Western Africa. Frontiers in Earth Science 9. doi: 10.3389/feart.2021.716630

Piccolo, A., Kaus, B.J., White, R.W., Palin, R.M., Reuber, G.S., 2020. Plume — Lid interactions during the Archean and implications for the generation of early continental terranes. Gondwana Research 88, 150–168. doi:10.1016/j.gr.2020.06.024.

Plomerová, J., Babuška, V., Dorbath, C., Dorbath, L., Lillie, R.J., 1993. Deep lithospheric structure across the Central African Shear Zone in Cameroon. Geophysical Journal International 115, 381–390. doi:10.1111/J.1365-246X.1993.TB01193.X.

Pysklywec, R.N., Cruden, A.R., 2004. Coupled crust-mantle dynamics and intraplate tectonics: Two-dimensional numerical and three-dimensional analogue modeling. Geochemistry, Geophysics, Geosystems 5. doi:10.1029/2004GC000748.

Ranalli, G., 1997. Rheology and deep tectonics. Annali Di Geofisica XL, 671–681. doi:10.4401/ag-3893.

Ranalli, Giorgio, and S.-I. Karato. "Rheology of the Earth." Tectonophysics 269, no. 3–4 (1995): 413. https://doi.org/10.1016/S0040-1951(96)00042-X.

Renne, P.R., Ernesto, M., Pacca, I.G., Coe, R.S., Glen, J.M., Prévot, M., Perrin, M., 1992. The Age of Paraná Flood Volcanism, Rifting of Gondwanaland, and the Jurassic-Cretaceous Boundary. Science 258, 975–979. doi:10.1126/SCIENCE.258.5084.975.

Stuart, G., Fairhead, J., Dorbath, L., Dorbath, C., 1985. A seismic refraction study of the crustal structure associated with the adamawa plateau and garoua rift, cameroon, west africa. Geophysical Journal International 81, 1–12. doi: 10.1111/j.1365-246X.1985.tb01346.x

Sykes, L.R., 1978. Intraplate seismicity, reactivation of preexisting zones of weakness, alkaline magmatism, and other tectonism postdating continental fragmentation. Reviews of Geophysics 16, 621–688. doi:10.1029/RG016i004p00621.

Tabod, C.T., Fairhead, J.D., Stuart, G.W., Ateba, B., Ntepe, N., 1992. Seismicity of the Cameroon Volcanic Line, 1982–1990. Tectonophysics 212, 303–320. doi:10.1016/0040-1951(92)90297-J.

Talwani, P. (Ed.), 2014. Intraplate Earthquakes. Cambridge University Press, Cambridge. URL: https://www.cambridge.org/core/books/intraplate-earthquakes/1590FD789B27385713896B23A2F7E6AC, doi:10.1017/CBO9781139628921.

Talwani, P., 2017. On the nature of intraplate earthquakes. Journal of Seismology 21, 47–68. doi:10.1007/s10950-016-9582-8.

Tanyileke, G.Z., Kusakabe, M., Evans, W.C., 1996. Chemical and isotopic characteristics of fluids along the cameroon volcanic line, cameroon. Journal of African Earth Sciences 22, 433–441. doi:10.1016/0899-5362(96)00025-5.

Tokam, A.P.K., Tabod, C.T., Nyblade, A.A., Julia, J., Wiens, D.A., Pasyanos, M.E., 2010. Structure of the crust beneath cameroon, west africa, from the joint inversion of rayleigh wave group velocities and receiver functions. Geophysical Journal International 183, 1061–1076. doi: 10.1111/j.1365-246X.2010.04776.x

Turcotte, D.L., Schubert, G., 2002. Geodynamics. Cambridge University Press. doi:10.1017/CBO9780511807442.

Vauchez, A., Tommasi, A., Barruol, G., 1998. Rheological heterogeneity, mechanical anisotropy and deformation of the continental lithosphere. Tectonophysics 296, 61–86. URL: https://linkinghub.elsevier.com/retrieve/pii/S0040195198001371, doi:10.1016/S0040-1951(98)00137-1.

Wang, H., Currie, C.A., 2017. Crustal deformation induced by mantle dynamics: Insights from models of gravitational lithosphere removal. Geophysical Journal International 210, 1070–1091. doi:10.1093/GJI/GGX209.

Wang, Y., Li, M., 2021. The interaction between mantle plumes and lithosphere and its surface expressions: 3-D numerical modelling. Geophysical Journal International 225, 906–925. URL: https://doi.org/10.1093/gji/ggab014, doi:10.1093/gji/ggab014.

Wegener, A., 1920. Die Entstehung Der Kontinente Und Ozeane. Friedr. Vieweg & Sohn.

Weiran, Y., Zuoxun, Z., Dewei, L., Jishan, X., Jie, W., Wenxing, L., 2009. Three-level Tectonic Model for Intraplate Earthquakes. Dixue Qianyuan/Earth Science Frontiers 16, 206–217. doi:10.1016/S1872-5791(08)60073-1.

Whattam, S.A., Stern, R.J., 2015. Late Cretaceous plume-induced subduction initiation along the southern margin of the Caribbean and NW South America: The first documented example with implications for the onset of plate tectonics. Gondwana Research 27, 38–63. doi:10.1016/j.gr.2014.07.011.

Willis, K., Houseman, G.A., Evans, L., Wright, T., Hooper, A., 2019. Strain localization by shear heating and the development of lithospheric shear zones. Tectonophysics 764, 62–76. doi:10.1016/j.tecto.2019.05.010.

CRediT authorship contribution statement

Almeida, J.: Model conceptualization and design, post-processing analysis, discussion of the results, writing of the manuscript. **Mohammadigheymasi, H.:** Seismic data collection and cataloging, discussion of the results, writing and review of the manuscript. **Neres, M.:** Model conceptualization, discussion of the results, writing and review of the manuscript. **Dumont, S.**: Model conceptualization, discussion of the results, writing and review of the manuscript.

Appendix I

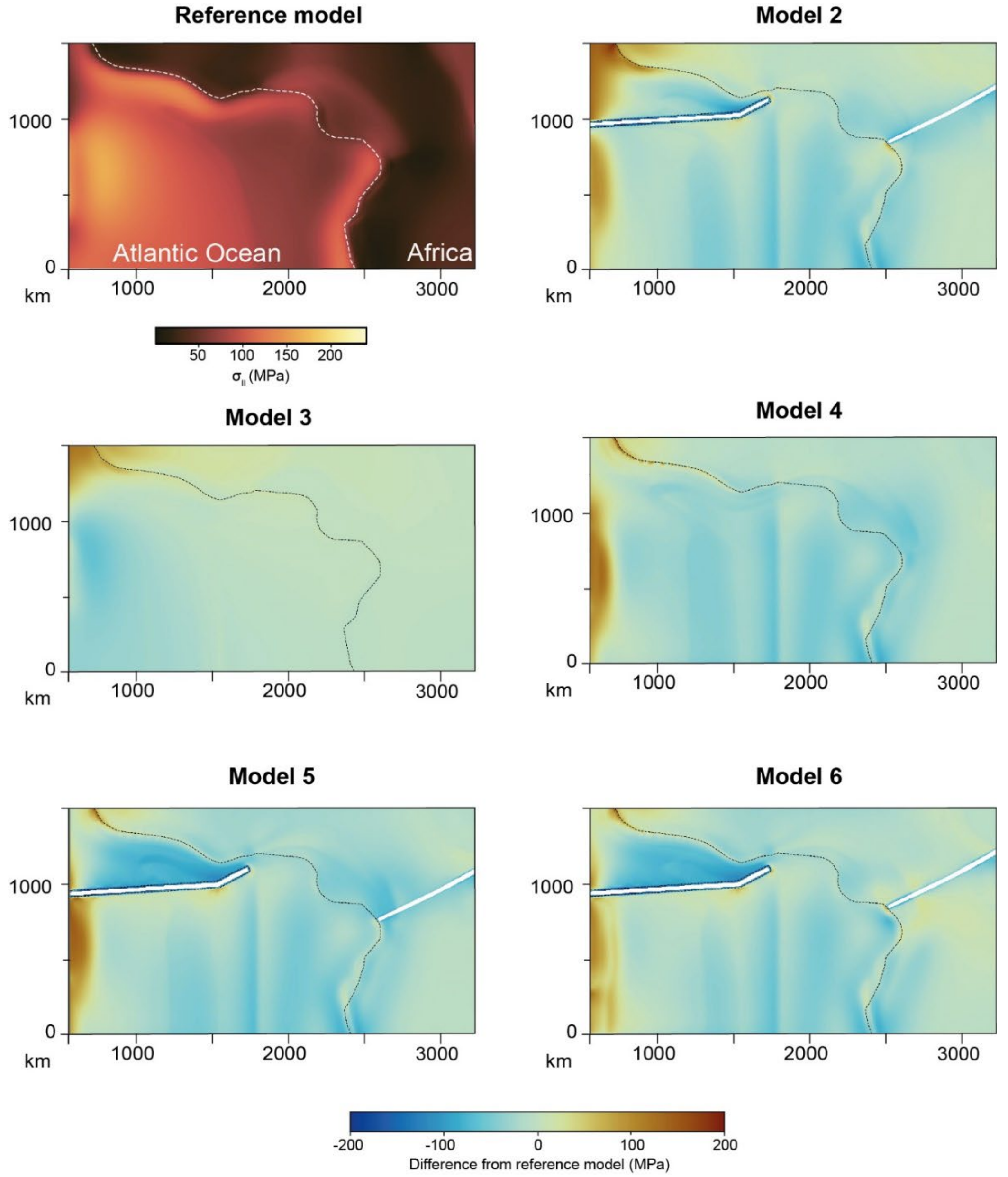

Supplementary Figure 1 – Variation in deviatoric stress magnitude (σ'_{II}) between models. This comparison allows for the clear observation of zones of stress “shadow” to the north of the Romanche weak zone, which result from its curved geometry.

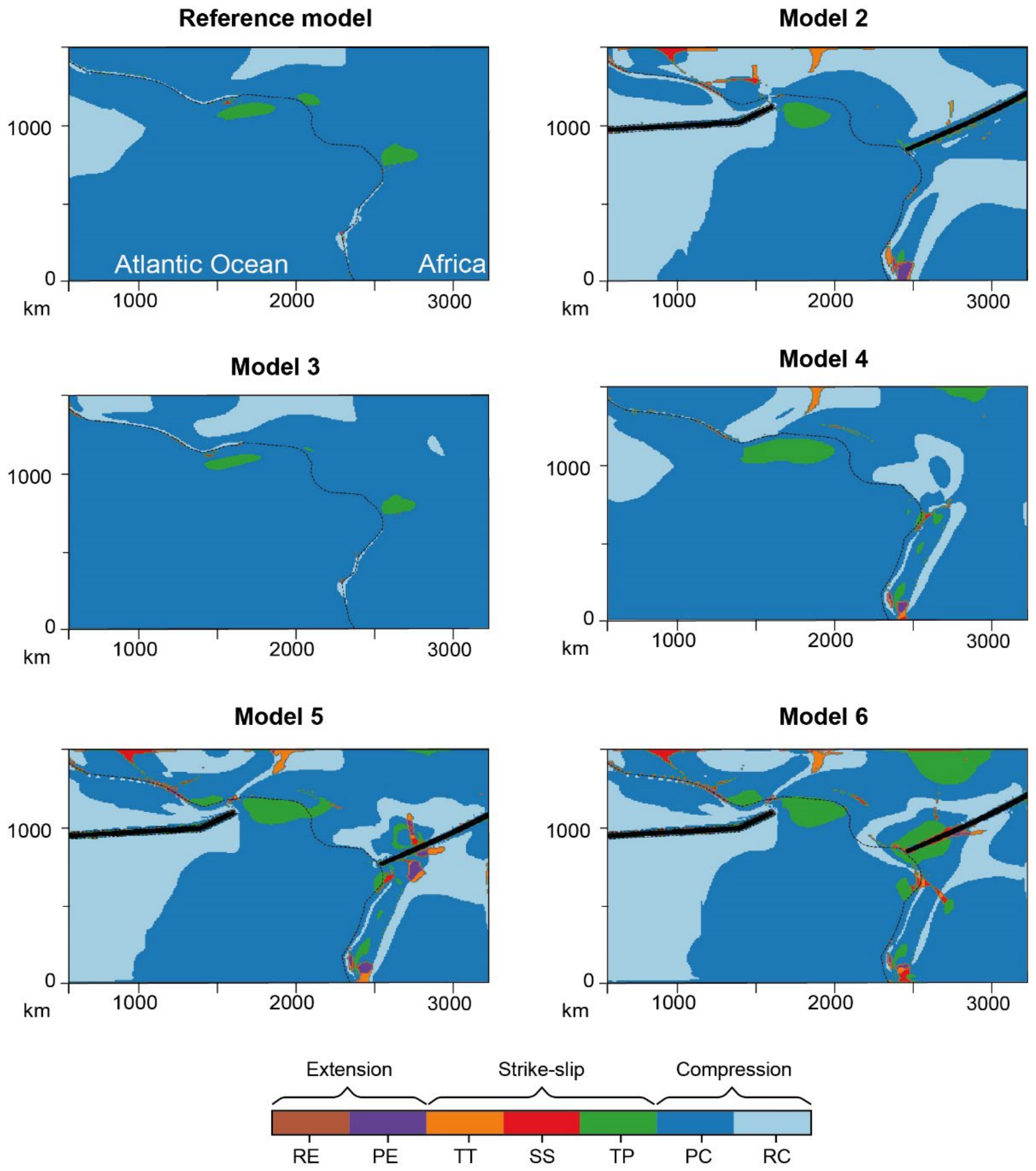

Supplementary Figure 2 – Final stress regimes for the different models. All models broadly predict compressive conditions for both the oceanic and continental plates, which is in-line with the known stress regimes for the region (e.g. Nkodia et al., 2022). It is noticeable that inflexion of the African coastline produces localized regions of transpression, indicating a strong influence from its shape on the overall deformation. Lastly, models with an active plume (Models 4, 5 and 6) show clear changes in the surface deformation imposed by the plume head.

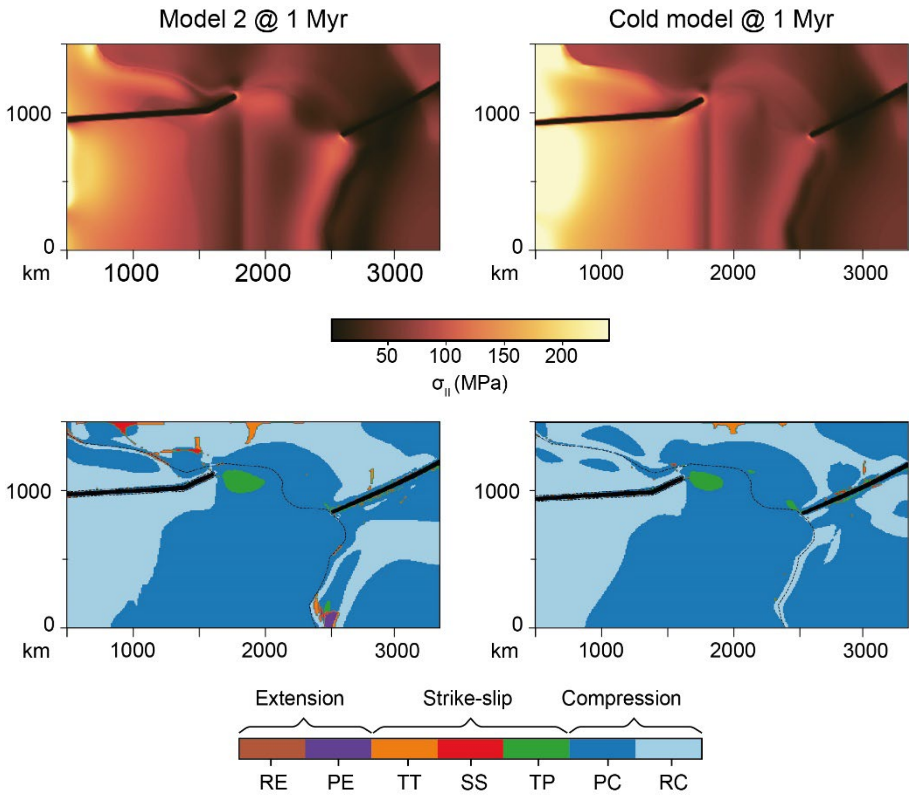

Supplementary Figure 3 – Comparison between Model 2 and a colder lithosphere model. The model on the right was created by taking Model 2 and doubling the initial thermal age of every continental lithosphere block. This further approximates the thermal profile to a geotherm (e.g., Chapman et al., 1997). While the generic pattern distribution is identical (i.e., a prevalence of compressional regimes), the second model loses most non-compressional sites. The older (and colder) regions of the model, located south of the CASZ are under pure compression, with the small extensional site disappearing.